Ultra High Energy Gamma Ray Astronomy at Akeno

P. G. Edwards, T. Kifune, *Institute for Cosmic Ray Research, University of Tokyo, Tanashi, Tokyo, 188 Japan*
M. Mori, *National Laboratory for High Energy Physics (KEK), Tsukuba, Ibaraki, 305 Japan*

Abstract: This paper describes the SPICA array at Akeno, and discusses recent efforts made to improve the angular resolution of the array, concentrating on the determination of the departure of the shower front from a plane. Future research plans are also outlined.

Introduction

Gamma rays with energies greater than 10^{14} eV are generally referred to as Ultra High Energy (UHE) gamma rays. The detection of UHE gamma rays from Cygnus X-3 marks the beginning of UHE gamma ray astronomy (Samorski and Stamm 1983a). UHE gamma rays have since been detected from a number of other objects, most of which are binary X-ray systems (see e.g. the review by Protheroe 1987). UHE gamma rays produce extensive air showers in the Earth's atmosphere, as do the much more numerous cosmic rays which form the background above which any UHE gamma ray signal must be detected. Extensive air showers are detected by arrays of detectors which use the fast-timing method to determine the direction of the incident particle or photon. At the Earth's surface, these showers consist mainly of a mixture of electrons, muons and gamma rays, spread laterally over ~ 100 m and longitudinally over ~ 1 m at the core increasing to >5 m beyond 100 m from the core.

UHE gamma ray emission is usually detected by the observation of a periodicity in the data which, in the case of binary X-ray sources, is consistent with an X-ray period. Any UHE gamma ray signal will obviously be easier to detect by reducing the background of cosmic ray showers. Improving the angular resolution of the array is the least controversial method of achieving this. The validity of using either the muon content of the shower or the age parameter of the lateral distribution fuction fitted to the data has yet to be conclusively proven (see e.g. Protheroe 1987).

The Akeno Observatory of the Institute for Cosmic Ray Research is located about 100 km west of Tokyo at an altitude of 900 m, corresponding to an atmospheric depth of 920 g cm^{-2}. The Observatory was established in 1975 with the construction of a 1 km^2 array (Hara *et al.* 1979). Since 1984 this has been extended with the construction of a 20 km^2 array, which will be part of a 100 km^2 array designed to study the highest energy cosmic rays ($E>10^{20}$ eV) (Teshima *et al.* 1986). In 1985 detectors were added to the central region of the 1 km^2 array to form the SPICA (SPecial Instrument for Cosmic ray Astrophysics) array, constructed specifically for UHE gamma ray astronomy. This array shares some detectors with the 1 km^2 array but has independent electronics and recording systems. The SPICA array originally consisted of one hundred and two 1 m^2 scintillator detectors, and this number has been gradually increased. At present the array consists of 132 detectors of which the outer 70 are used for density measurements only, 52 are used for both density and timing, and 12 are used for timing only. Nearly all detectors have the scintillator viewed from 1 m above

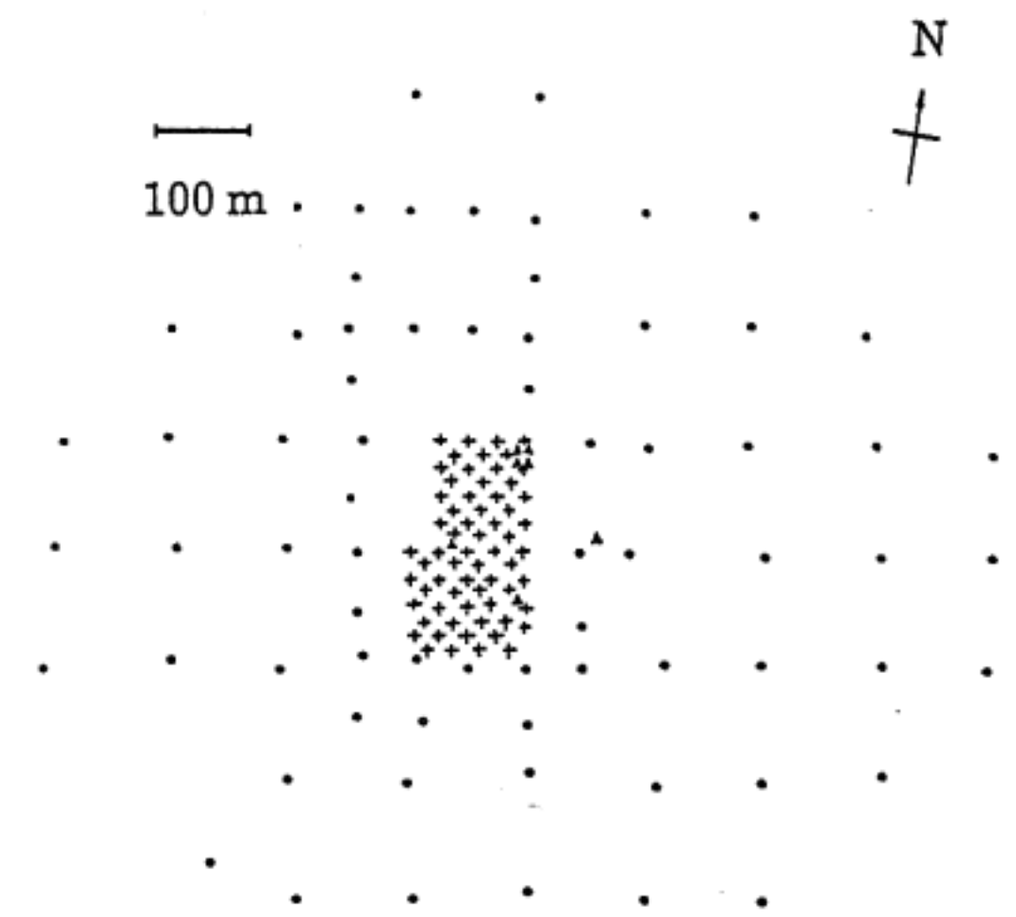

Figure 1—The layout of the SPICA array. Circles represent detectors used for density measurements only. Crosses represent detectors used for fast-timing. Triangles represent muon detectors. The 28 northern fast-timing detectors make up the S21 and S23 sub-arrays. The S41 and S44 sub-arrays are made up from the southern 36 fast-timing detectors.

by either a 2″ or 5″ photomultiplier. The SPICA array originally consisted of two separated fast-timing areas, each further divided into two overlapping, but independent, sub-arrays. Data from all four sub-arrays were recorded when any one of the four sub-arrays was triggered. The position of the detectors and sub-arrays are shown in Figure 1. Three of the sub-arrays use 'home-made' electronics (S21, S23, S41), while the fourth (S44) uses a CAMAC system. This system is still in use, although the original CAMAC system has been expanded to include all the S41 and S44 detectors (i.e. all those in the southern area), and a new CAMAC system combining all the S21 and S23 detectors has been added. Most detectors are thus part of 2 of the total of 5 sub-array configurations.

Shower Front Curvature

Our first step in determining the angular resolution was to gauge the importance of including shower front curvature in the shower analysis. Shower front curvature has been known to exist for many years, however, particular for arrays of limited extent, the plane front approximation has generally been used. (As we shall see, 'departure from a plane' is a more precise description of this effect than 'curvature', however the latter is more commonly used and will be used here.) We first considered showers with cores falling between the S23 and S41 areas, and examined the directions obtained by fitting plane shower fronts to the S23 and S41 sub-array data. The SPICA array runs approximately north-south and, to a first approximation, comparing the declinations obtained by the two separate analyses serves as a good check of the accuracy of the plane shower front fit. It was found that the declination of showers triggering S23 was less than that of S41 in 99% of cases. This result is consistent with curvature, and so we undertook a more careful analysis of these events. The direction cosines from the two directions were averaged and renormalized to obtain the 'best' direction. The offset of each detector in both S23 and S41 from the plane normal to this direction and passing through the core was found as a function of core distance (i.e. perpendicular distance from the shower axis). This procedure

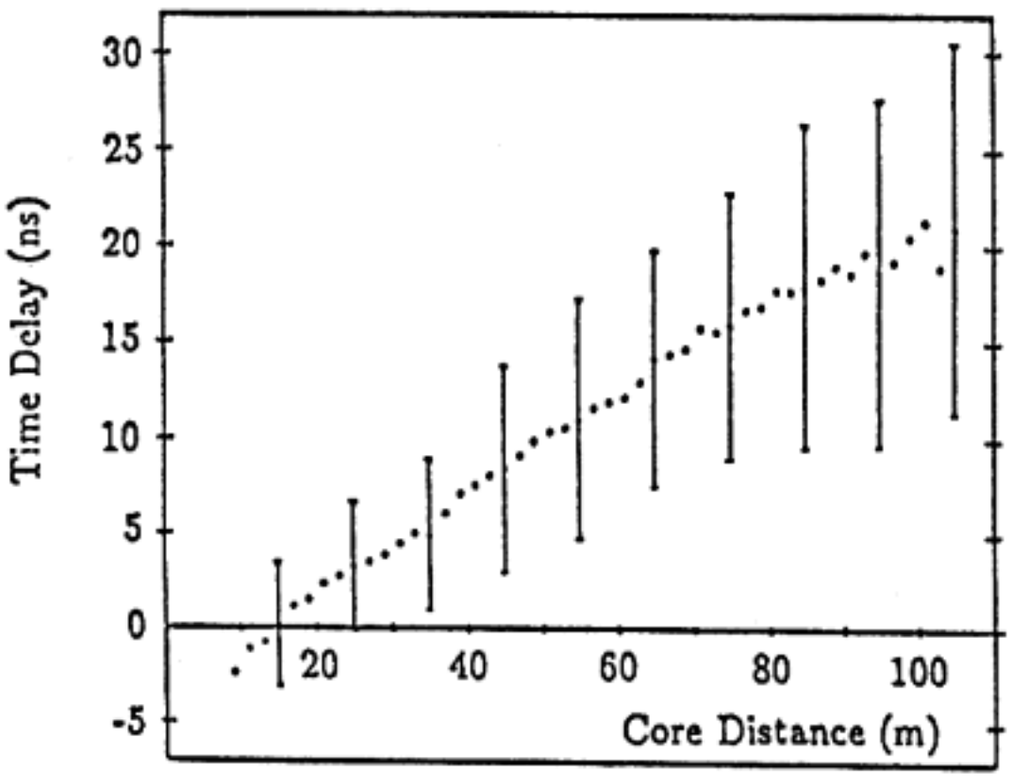

Figure 2—The average time delay from a plane shower front as a function of core distance. Representative $\pm 1\sigma$ error bars are shown. All points are the average of at least 50 values.

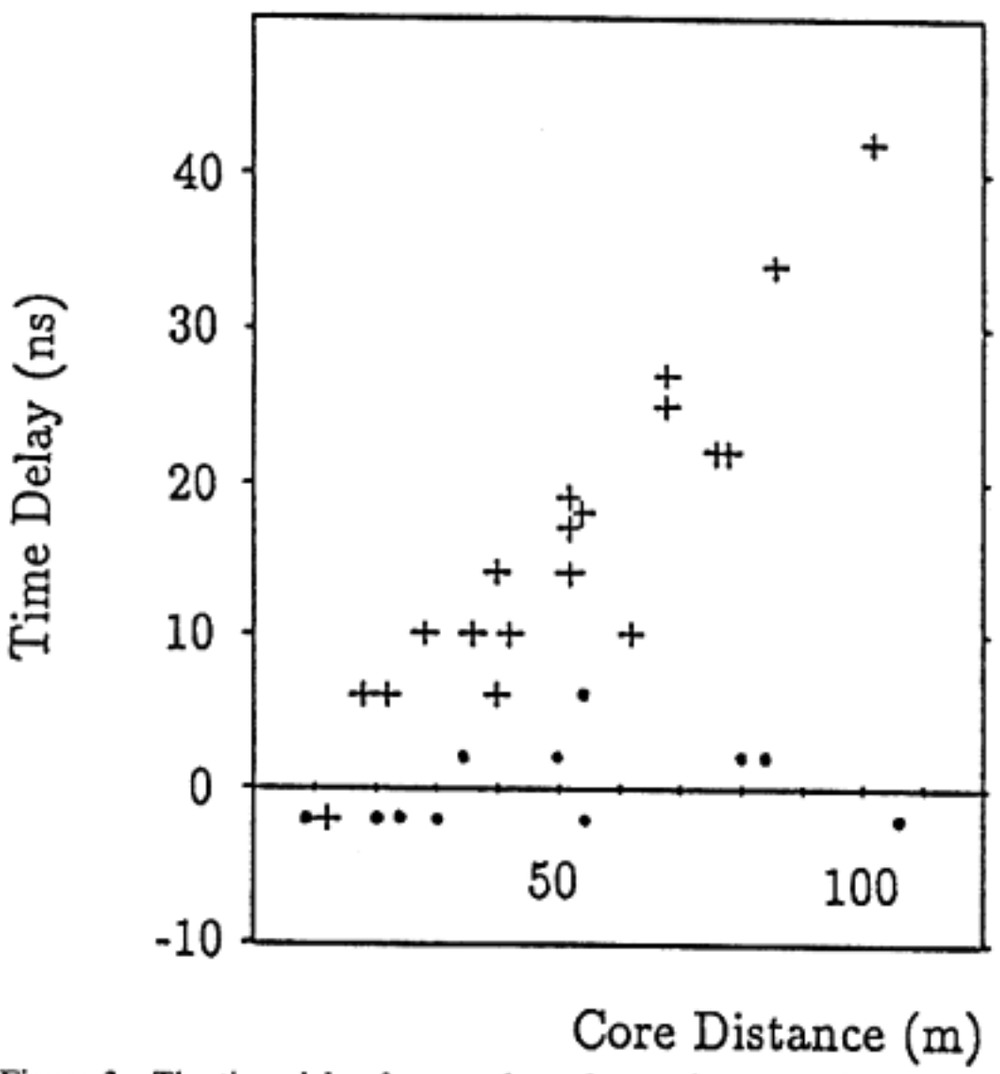

Figure 3—The time delay from a plane shower front as a function of core distance for two events, showing the range of fluctuation from event to event.

was repeated for >1500 events, and the resulting plot of average time delay against core distance is shown in Figure 2. It is immediately apparent that the spread of points is quite large, and increases with core distance. Two individual events are shown in Figure 3. These are atypical events in that their curvatures lie towards the extremes of Figure 2, but their self-consistency indicates that a major contribution to the spread in Figure 2 results from fluctuations in individual showers. Also, as core distance increases the particle density decreases and the shower thickness increases resulting in a larger spread further from the core. Figure 2 also illustrates that the simple model of a single radius of curvature is not valid.

The time delay—core distance relation was also determined after dividing the data into several size ranges. With increasing shower size, the spread of data points decreases slightly, and there is also a tendency for the average time delay for a given core distance to decrease, i.e. larger showers are marginally flatter. However, as the average variation of each size range from the overall average is <1 ns, the average distribution is presently used for all size ranges.

It is in principle possible to determine the curvature of each event in the analysis procedure, however this would be very time consuming. We prefer instead to use the average curvature obtained from Figure 2 to correct all showers. The negative delay closest to the core that is evident in Figure 2 was unexpected. Three possible interpretations can be made of this region. It may result from some real property of the shower front, i.e. the core may be more advanced with respect to the rest of the shower front than expected. Alternatively it may indicate that the highest densities near the core are causing the photomultipliers in these detectors to trigger during the passage of the particles through the photomultiplier. Photomultipliers are usually triggered by light produced as the shower front passes through the scintillator. Thus, should this effect be real, the apparent relative advance of the core region should be twice the separation from the photomultiplier to the scintillator i.e. about 6 ns—which is in reasonable agreement with the data. The third possibility is that this effect is an artefact of the analysis procedure, although we consider this unlikely. Investigation of this effect is continuing.

These results may be compared with those of others. The large spread we find in the data is consistent with the results of Bennett *et al.* (1962), who determined the radius of curvature for each of ~1200 events, and found that the value fluctuated greatly from event to event. Linsley and Scarsi (1962) showed that a single value for the radius of curvature did not describe a shower well, and that the curvature decreased (i.e. the radius of curvature increased) with increasing core distance, again in qualitative agreement with the present results. As these two experiments were performed with arrays covering a much larger area than the SPICA array no direct comparison can be made. Woidneck and Böhm (1975), using the Kiel array, found that the distribution of time delays at ~50 m from the core is different from the distribution near the core, and attributed the change to a larger contribution of muons at larger core distances which arrive earlier than the electrons. An earlier result from the Kiel arrays gives the departure from a plane front for core distances <63 m (Woidneck *et al.* 1971). The Kiel array is situated at sea-level and, as the naive model of a single radius of curvature for a shower would lead us to expect, their results indicate a slightly flatter shower front (i.e. larger radius of curvature) than our results, although the large fluctuations in our data preclude any definite conclusions. The results of Eames *et al.* (1987) from the Haverah Park array, situated 200 m above sea level, also show a smaller curvature than our results. However, their results seem to imply a much stronger flattening with shower size than we observe.

Angular Resolution

Once the correction for shower front curvature had been determined, we were able to calculate the angular resolution of the array. The angular resolution is proportional to the baseline over which timing information is obtained. Two approaches were adopted to determine the angular resolution. Both involved dividing the S44 sub-array in two, finding the direction of a shower with each half, and comparing the resulting directions. The first method is usually referred to as the odd-even method, as it uses alternate detectors for the two halves. This method has the advantage that the overall baseline is the same as that of the whole array. The second approach is to

Table 1

Dependence of Angular Resolution on Data Cuts

Cut made to data	Number of events	Angular resolution figure of merit : Odd-Even method (°)	Core-centre split (°)
Curvature correction			
No correction	4650	1.29	3.18
Modified Linsley	4700	0.98	1.87
Our result	4900	0.95	1.26
Core acceptance area			
60 m x 65 m	2300		1.15
100 m x 105 m	4750		1.26
140 m x 145 m	6050		1.31
No core cut	7250		1.39
Zenith angle (θ)			
$0° < \theta < 17°$	1650	0.90	1.20
$17° < \theta < 25°$	1400	0.93	1.28
$25° < \theta < 40°$	1750	1.04	1.34
Size and nft			
No size or nft cut	100%	0.95	1.26
Low size cut	66%	0.88	1.15
High size cut	33%	0.79	1.04
Low nft cut	66%	0.83	1.11
High nft cut	33%	0.73	0.96

Unless the parameter is being varied, the analysis was performed for events with zenith angles < 40°, a core acceptance area of 100 m x 105 m, with no size or nft cuts, and using our curvature correction. No values were obtained for core acceptance area cuts using the odd-even method. The values quoted for the size and nft cuts are interpolated values to allow a more direct comparison with each other. Errors in the values given are expected to be ~ 3 %.

divide the array with a line passing through the core of a shower and the geometrical centre of the array. This method of splitting will obviously vary from event to event. Although the overall baseline is reduced in this approach, the advantage of this method is that it is a good test of the effect of the curvature correction on the analysis. The first method tests the reproducibility of finding the direction, whereas the second method checks the accuracy of the direction. With the usual assumption that the errors in the two sub-arrays add in quadrature and that the angular resolution improves as the square root of the number of detectors, the resultant angular resolution for the array is half that obtained by these methods. Various cuts are made to the data before the angular resolution is checked. These cuts—which exclude events with large zenith angles, large core distances or bad fits to the timing or density information—are the same as those that will be made when searching for UHE gamma rays. The angle between the directions from the two sub-arrays is initially plotted as a histogram. In the following discussion the median of this distribution is used as the relative figure of merit. Its relation to the final angular resolution is discussed later.

We first found the angular resolution as a function of the curvature correction. Analyses with (a) no curvature correction, (b) a modified form of a correction due to Linsley (1985) and (c) our empirical correction were trialled, the results of which are presented in Table 1. As expected the second method of

analysis is much more sensitive to the type of curvature correction employed. The modified Linsley formula is derived from data at much larger core distances (and therefore larger shower sizes) than the present array, and it is thus not surprising that it is not as accurate at smaller core distances. For both methods our empirical fit gives the best results. The angular resolution was also investigated as a function of zenith angle, core acceptance area, size and number of fast-timing detectors triggered (hereafter nft). These results are also summarised in Table 1. The angular resolution worsens slightly with increasing zenith angle, and also as the core acceptance area is increased. The largest effect however is found by applying cuts to the size and nft. These two quantities are obviously closely related as, particularly for showers with cores near the centre of the sub-array, a larger size will trigger more detectors. However, as indicated in Table 1, nft cuts showed a more significant improvement than the cuts in size, emphasizing the basic dependence of angular resolution on the timing baseline. Although large improvements to the angular resolution can be made by imposing size or nft cuts, it is only with the loss of a considerable number of events. It is, however, quite feasible in searching for UHE gamma rays to perform analyses for several size/nft ranges and use the appropriate angular resolution for each range.

All the preceding analysis was performed with the 32 detectors of the S44 sub-array which contains 32 detectors. As the dimensions, number of detectors and thresholds of each sub-array differ, we expect a corresponding slight difference in the angular resolution of each sub-array. For the S44 sub-array in particular, the angular resolution will also be time-dependent, as the expansion of this sub-array has occurred over many months. Calculations of the angular resolution for each sub-array are continuing.

For the purpose of the previous discussion, the median of the angular spread distribution was used. However in the analysis of data from a point source, we wish to optimize any on-source signal against the isotropic cosmic ray background. The array angular resolution (i.e. the angular spread distribution expressed per solid angle) can be fitted by a Gaussian distribution, in which case the optimum angle is a factor of 1.59 larger than the standard deviation of this distribution. Within this solid angle, 72% of events from a point source would be expected to arrive. This optimum angle is a function of zenith angle. To a first approximation, this may be treated by modifying the acceptance angle for a given object by a factor depending on its declination (see Protheroe and Clay 1984).

Muon Collection Area

Early theoretical studies suggested that the muon content of gamma ray initiated showers would be at least an order of magnitude smaller than that of cosmic ray initiated showers. In contrast the electron number for the two kinds of showers is expected to be approximately equal. The original observations of Samorski and Stamm (1983b) with the Kiel array implied that the muon content of gamma ray initiated showers was only slightly less than that of cosmic ray showers. The observation of Cyg X-3 with the Akeno 1 km^2 array showed the most significant correlation with the 4.8 hr binary period for showers with an muon to electron ratio less than one thirtieth of that of normal showers (Kifune *et al.* 1986). Theoretical calculations have also supported the conventional belief (e.g. Edwards *et al.* 1985). However, more recent observations of UHE gamma ray bursts from her X-1 by the Los Alamos group (Dingus *et al.* 1988), and theoretical models assuming higher photo-pion cross-sections (Drees *et al.* 1988) support the observations of Samorski and Stamm. Clearly the situation is far from resolved, and observations with a large muon collection area are very desirable.

The 1 km^2 array has ten 25 m^2 muon stations distributed over the array area. The SPICA system initially used only one of these stations, but in January 1987 four more stations were added. In June 1988 this was further extended, so that now a total of 175 m^2 muon collecting area is available. This is compared to the collecting areas of 21 m^2 for the Kiel experiment and 44 m^2 at Los Alamos. All muon stations consist of fifty 5 m × 10 cm × 10 cm proportional chambers filled with P10 gas (90% Argon, 10% Methane) (Hayashida and Kifune 1980). Five stations are covered by a 2 m thickness of concrete to absorb the electrons and photons, resulting in a muon threshold energy of 1 GeV. The remaining two stations are shielded by 1 m of concrete and have a 0.5 GeV threshold. A 90 m^2 muon calorimeter has also been used in the 1 km^2 array in the past, but at present this is being used in a separate slow monopole search experiment (Hara *et al.* 1986). At the conclusion of this experiment it is anticipated that this detector will be added to the SPICA array.

Observing Program

The SPICA array started operation in December 1985 and has run almost continuously ever since, giving a good, uniform coverage of the sky. Preliminary results for Cyg X-3 from the first years operation were presented by Kifune *et al.* (1987). The two and a half years data collected so far is currently being reanalysed to take the shower front curvature into account. Several other improvements have been made to the analysis procedure, resulting in a more accurately determined core position and shower size. It is planned to search for UHE gamma-ray emission from a number of gamma and X-ray sources. These include the confirmed UHE gamma ray sources Cyg X-3 and Her X-1, and others from which UHE gamma ray emission has been claimed, such as the black hole candidate Cyg X-1 (Fomin *et al.* 1987). A clock capable of 100 μs accuracy has been installed at Akeno, also allowing searches to be carried out at pulsar periods.

Acknowledgements

PGE gratefully acknowledges the support of a Monbusho scholarship. This analysis was performed with the computer of the Institute for Nuclear Study, University of Tokyo. This work is supported by Monbusho (the Ministry of Education, Science and Culture).

Bennett, S., Delvaille, J., Greisen, K. and Kendziorski, F., 1962, *J. Phys. Soc. Japan.*, **17**, Suppl. A-III, 196.
Dingus, B. L. *et al.*, 1988, *Phys. Rev. Lett.*, (submitted).
Drees, M., Halzen, F. and Hikasa, K., 1988, preprint.
Eames, P. J. V. *et al.*, 1987, *Proc. 20th International Cosmic Ray Conference (Moscow)*, **2**, 449.
Edwards, P. G., Protheroe, R. J. and Rawinski, E., 1985, *J. Phys. G: Nucl. Phys.*, **11**, L101.
Fomin, Yu.A. *et al.*, 1987, *Proc. 20th International Cosmic Ray Conference (Moscow)*, **1**, 397.
Hara T. *et al.*, 1979, *Proc. 16th International Cosmic Ray Conference (Kyoto)*, **8**, 135.
Hara T. *et al.*, 1986, *Phys. Rev. Lett.*, **56**, 553.
Hayashida, N. and Kifune, T., 1980, *Nucl. Instr. Meth.*, **173**, 431.
Kifune, T. *et al.*, 1986, *Astrophys. J.*, **301**, 230.
Kifune, T., Mori, M., Hara, T. and Nishijima, K., 1987, in Very High Energy Gamma Ray Astronomy ed. K. E. Turver (D. Reidel), 173.
Linsley, J., 1985, *Proc. 19th International Cosmic Ray Conference (La Jolla)*, **3**, 461.

Linsley, J. and Scarsi, L., 1962, *Phys. Rev.*, **128**, 2384.
Protheroe, R. J., 1987, *Proc. 20th International Cosmic Ray Conference (Moscow)*, **8**, 21.
Protheroe, R. J. and Clay, R. W., 1984, *Proc. Astron. Soc. Aust.*, **5**, 586.
Samorski, M. and Stamm, W., 1983a, *Astrophys. J. Lett.*, **268**, L17.
Samorski, M. and Stamm, W., 1983b, *Proc. 18th International Cosmic Ray Confernece (Bangalore)*, **11**, 224.
Teshima, M. *et al.*, 1986, *J. Phys. G: Nucl. Phys.*, **12**, 1097.
Woidneck, C. P. and Böhm, E., 1975, *J. Phys. A: Math. Gen.*, **8**, 997.
Woidneck, C. P., Böhm, E., Trümper, J. and de Villiers, E. J., 1971, *Proc. 12th International Cosmic Ray Conference (Hobart)*, **3**, 1038.